chemosensors

MDPI

Article

Preparation, Characterization and Electrochemical Response of Nanostructured TiAlV with Potentiostatically Deposited IrOx as a pH Sensor for Rapid Detection of Inflammation

Jitřenka Jírů [1], Vojtěch Hybášek [1], Alena Michalcová [1], Klára Korbelová [1], Lukáš Koláčný [2] and Jaroslav Fojt [1,*]

[1] Department of Metals and Corrosion Engineering, University of Chemistry and Technology Prague, Technická 5, 166 28 Prague, Czech Republic; jiruj@vscht.cz (J.J.); hybasekv@vscht.cz (V.H.); michalca@vscht.cz (A.M.); korbelok@vscht.cz (K.K.)

[2] Department of Organic Technology, University of Chemistry and Technology Prague, Technická 5, 166 28 Prague, Czech Republic; kolacnyl@vscht.cz

* Correspondence: fojtj@vscht.cz

Abstract: Electrochemical pH sensors have a wide range of industrial applications such as in medicine due to their fast response and high sensitivity to pH changes. This work focuses on the preparation of samples based on the nanostructure of TiO_2 with potentiostatically deposited particles of iridium and its oxides (IrO_2), using a Ti-6Al-4V alloy as the base material, and subsequent surface characterization. Transmission electron microscopy and secondary ion mass spectroscopy showed Ir particles distributed in the nanotubes. Using a potentiostatic method, a stable pH sensor was prepared. By monitoring the open circuit potential, it was shown that this sensor is usable even without being kept in a storage medium and does not react to changes in the redox potential of the solution.

Keywords: pH sensor; Ir oxide; implant; electrochemistry; titanium

Citation: Jírů, J.; Hybášek, V.; Michalcová, A.; Korbelová, K.; Koláčný, L.; Fojt, J. Preparation, Characterization and Electrochemical Response of Nanostructured TiAlV with Potentiostatically Deposited IrOx as a pH Sensor for Rapid Detection of Inflammation. *Chemosensors* **2024**, *12*, 109. https://doi.org/10.3390/chemosensors12060109

Received: 17 May 2024
Revised: 7 June 2024
Accepted: 10 June 2024
Published: 11 June 2024

1. Introduction

Infection is one of the possible causes of implant failure in the human body. As with all invasive surgical procedures, arthroplasty is not completely risk-free. Medical device-associated infection is a worldwide health problem because it is very difficult to diagnose, very difficult to treat and very expensive to treat. The complexity of diagnosing these infections adds to the challenge, often relying on clinical symptoms reported by patients, such as pain, swelling, or compromised joint mobility. However, these symptoms can be non-specific and may overlap with other post-operative complications, necessitating a comprehensive evaluation for accurate diagnosis. Moreover, infection detection often relies on non-specific markers such as elevated leukocyte count and heightened C-reactive protein (CRP) levels, further complicating the diagnostic landscape [1–3]. The efficacy of antibiotic therapy is also a growing concern, given the emergence of antibiotic-resistant strains, posing significant challenges in infection management. Despite the administration of comprehensive treatment, infections often result in surgical removal of the implant. It is also associated with a high mortality of patients [4–6].

The spread of infection occurs due to the preference of bacteria to exist on the implant surface in established communities known as biofilms. Biofilm formation occurs by the attachment and aggregation of free-floating bacteria on the implant surface. The bacteria that exist in the biofilm are part of a complex multicellular community enclosed in extracellular polymeric substances (EPSs). The EPSs produced by the bacteria form a 'slime layer' around the cells, consisting mainly of water and a range of polysaccharides, nucleic acids, proteins and lipids. Bacterial biofilms can resist antibiotics, disinfectants, phagocytosis and other components of the host's innate and adaptive immune system. The main microorganisms that cause infection and subsequent inflammation include *Staphylococcus aureus*,

S. epidermidis and *S. hominis*, among others. Infecting organisms can be implanted with biomaterials into the body [1,7,8]. These bacteria are known to produce acid metabolites, including lactic acid, which exert a significant impact on the pH levels of the surrounding tissue [9,10].

The pH value stands as a pivotal parameter across numerous domains including industry, agriculture, biology, environment and medicine. Traditionally, pH determination has relied on the utilization of glass electrodes. However, despite its widespread use, the glass electrode method presents several drawbacks. High impedance, significant cost, bulky dimensions, restricted shape versatility and susceptibility to mechanical damage are among the primary limitations associated with this conventional approach. These constraints not only impede the widespread deployment of pH measurement systems but also hinder their adaptability to diverse environmental and operational conditions. Consequently, the exploration of alternative pH sensing technologies has emerged as a critical endeavor, aiming to overcome these limitations and deliver more robust, cost-effective and versatile solutions for pH monitoring across various applications [9,11–14].

Over the past two decades, a primary objective has been the exploration of materials with the potential to serve as effective pH sensors. Notably, metal oxide (MOx) electrodes have emerged as promising candidates due to their ability to respond to changes in pH [15]. Unlike traditional glass electrodes, MOx electrodes offer the advantage of adjustability in dimensions, addressing concerns related to size and shape limitations. Consequently, researchers have extensively investigated various MOx electrodes, including titanium dioxide (TiO_2), aluminium oxide (Al_2O_3), platinum dioxide (PtO_2), iridium dioxide (IrO_2) and tungsten trioxide (WO_3), among others, for their suitability as pH sensors. These investigations have revealed promising properties of MOx electrodes, including enhanced sensitivity, improved stability and greater versatility, positioning them as viable alternatives to conventional pH measurement technologies [16–22].

TiO_2 thin film is an n-type semiconductor renowned for its exceptional chemical stability, rendering it a promising candidate for pH sensing applications, particularly in highly acidic or alkaline solutions. Its inherent qualities include excellent chemical stability, making it a sought-after material in various industrial and biomedical contexts. TiO_2 boasts a reputation for being non-toxic, environmentally friendly and corrosion-resistant, further enhancing its appeal for diverse applications. Of particular note is its remarkable biocompatibility, making it invaluable for medical applications, where materials must interact safely with biological systems [23,24]. Moreover, TiO_2 exhibits unique ionic and electrical properties, distinguishing it from other oxides and amplifying its utility in sensor technologies. Multiple fabrication techniques exist for producing TiO_2 nanostructures, among which sol–gel and electrochemical methods are prominent [22,23,25].

IrO_2, among the array of metal oxides considered for pH sensing, has emerged as a standout candidate due to its remarkable stability across a broad pH spectrum, even under high-pressure conditions and in aggressive environments. Notably, IrO_2 exhibits rapid response characteristics, even in non-aqueous solutions, making it exceptionally versatile for various pH measurement applications. Crystallizing in a rutile structure akin to that of ruthenium dioxide (RuO_2), IrO_2 demonstrates a lower catalytic activity compared to RuO_2. Despite this distinction, IrO_2-based electrodes have garnered considerable attention, particularly in biomedical contexts, owing to their impressive stability and performance metrics [11,19–21].

In numerous biomedical applications, iridium oxide-based electrodes have proven invaluable. Compared to other materials such as antimony, titanium, ruthenium or palladium-based electrodes, iridium oxide layers offer distinct advantages. These include faster response times across a wide pH range and superior biocompatibility, underscoring their suitability for interfacing with biological systems. The utilization of IrO_2 electrodes not only enhances the precision and reliability of pH measurements but also aligns with the stringent requirements of biomedical applications, where accuracy and compatibility are paramount considerations [6,14,16,22,25].

In this work, the main objective was to reproducibly create a pH sensor based on TiO_2 nanotubes with deposited iridium. This prepared sensor could one day be part of an implant for the rapid detection of inflammation, and subsequently, its surface could be characterized and its electrochemical response to pH change could be investigated. The use of this sensor without the need for a storage medium was also tested. The use of a metal sensor without a storage medium would reduce two disadvantages of conventional glass pH electrodes.

2. Materials and Methods

As a base material, the Ti-6Al-4V ELI alloy (extra-low interstitials, Ti grade 23) was selected. The diameter of the samples was 16 mm and the height was 3 mm. The surface was ground with a series of abrasive papers up to FEPA 2500 grit. The samples were then rinsed with distilled water, ethanol and acetone. By anodic oxidation, the surface of the prepared samples was nanostructured in a solution of 1 mol/L $(NH_4)_2SO_4$ (Lach:ner, Neratovice, Czech Republic) and 0.2 wt.% NH_4F (Lach:ner) in a PTFE cell. A standard three-electrode setup consists of a silver/silver chloride electrode (3 mol/L KCl, further labeled as SSCE), a glassy carbon counter electrode, and the sample as the working electrode. The nanostructure preparation process consisted of two parts: in the first part, the potential was increased to 20 V/SSCE at a rate of 100 mV/s, and the second part was potentiostatic for 2200 s. The nanostructured alloy was subsequently cleaned in distilled water and ethanol in an ultrasonic cleaner and dried with hot air.

For the deposition of iridium oxide on the nanostructured Ti-6Al-4V surface, a solution of 0.2 mmol/L $IrCl_3 \cdot xH_2O$ (Sigma-Aldrich, St. Louis, MO, USA), 1 mmol/L $C_2H_2O_4 \cdot 2H_2O$ (oxalic acid, Lach:ner) and 5 mmol/L K_2CO_3 (Lach:ner) was used. The solution was aged for 4 days at 37 °C and stored at 5 °C prior to use. The deposition was carried out using potentiostatic mode (−0.4 V/SSCE, 7200 s; further labeled as Ir PS) with an exposure area of 1 cm^2, and the three-electrode setup was used. After deposition, the samples were ultrasonically cleaned in distilled water.

Nanostructured Ti-6Al-4V and Ir PS underwent an oxidation by cyclic polarization (E_{OCP} = 3400 s, −0.05 V/E_{OCP} to 0.1 V/E_{OCP} and back to 0.01 V/E_{OCP}, 20 cycles) in a physiological solution (9 g/L NaCl, Lach:ner). These samples will be further labeled as TiAlV and Ir PS+CP.

Scanning electron microscopy (SEM, TESCAN MIRA 3 LMU with OXFORD INCA 350 EDS analyzer, Brno, Czech Republic) was used for the morphological analysis of the prepared samples. Further analysis was performed using a transmission electron microscope (TEM, EFTEM Jeol 2200 FS, Tokyo, Japan). Samples for TEM (lamellas) were created using SEM (TESCAN LYRA 3, Brno, Czech Republic) and a focused ion beam (FIB) using gallium ions. Secondary ion mass spectroscopy (SIMS) was measured on the same SEM. Image analysis was performed manually using Image J 2.15.0 software.

Electrochemical measurements were realized with potentiostat Gamry Instrument Reference 600 (Warminster, USA) at 37 °C, with the same setup as mentioned earlier, with an exposed area of 1 cm^2. For pH changes, a physiological solution (9 g/L NaCl) with biological buffer TES (N tris(hydroxymethyl)methyl-2-aminoethanesulfonic acid, 5.9 g/L, Sigma-Aldrich, St. Louis, MO, USA) was used. For pH changes, a scale of 7.6, 7.4, 7.0 and 6.5 was chosen and the pH was adjusted with diluted NaOH. The electrochemical response of the prepared samples to the pH change was detected using the monitoring of open circuit potential (E_{OCP}). In order to investigate the effect of the redox potential of the system on the detection of pH change, measurements were performed with a platinum electrode as the working electrode and a silver chloride electrode as the reference electrode. At the same time, a sample was connected in the same cell as the working electrode and a silver/silver chloride electrode as a reference. During the measurement, the solution at pH 7.6 and 6.5 was bubbled first with N_2 and then with air. The potential recording was carried out simultaneously on two potentiostats.

3. Results and Discussion

3.1. Base Material

A nanotubular TiO_2 structure was formed on the Ti-6Al-4V surface by anodic oxidation in a fluoride solution. This procedure was consistent with published procedures [26,27]. The surface morphology is shown in Figure 1. It can be seen that the nanostructure is not homogenous as dissolved regions of the β-phase are present, which is due to the fact that this phase is richer in vanadium than the α-phase, which is richer in aluminum [28]. In a fluoride environment, vanadium dissolves faster than aluminum, this leads to a faster dissolution of the β-phase and the formation of nanotubes is not uniform.

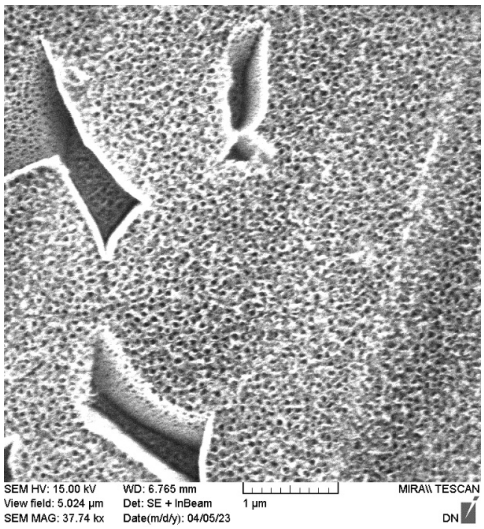

Figure 1. Native 20V TiO_2 nanotubes on the Ti-6Al-4V alloy.

After surface preparation, the sample was further oxidized by cyclic polarization, the course of cyclic polarization is shown in Figure 2a. The TiAlV sample was immersed in the physiological solution at pH 7.6 and the potential course was monitored (Figure 2b). During this time, the nanotubes were flooded and hydrated compounds formed on their surface. This process took 6 days, after which the sample was put into solutions of different pH and the electrochemical response was monitored. The result is shown in Figure 3. TiAlV exhibited a sub-Nernstian response of 31 ± 1 mV/pH.

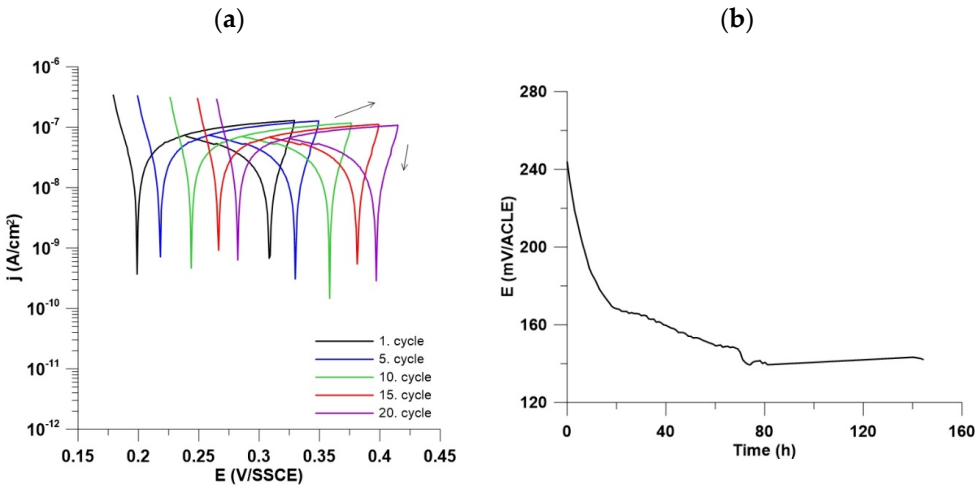

Figure 2. (**a**) The current and potential dependencies of oxidation of TiAlV, arrows indicating polarization direction; (**b**) the process of the potential stabilization of the TiAlV in physiological solution at pH 7.6 at 37 °C.

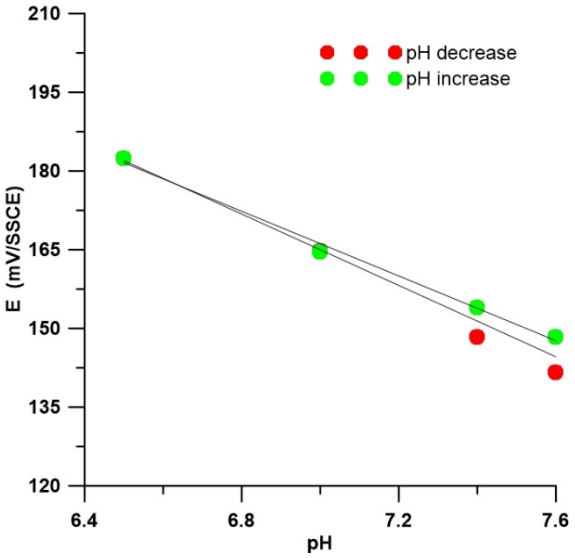

Figure 3. Results of potential change in pH change for TiAlV in physiological solution at 37 °C.

3.2. Sample Preparation and Characterization

The fresh solution of Ir was yellow, but after 4 days of aging at 37 °C, the color changed to blue, still having pH 10. This corresponded to the formation of iridium complexes in the solution, which are in line with the outcomes of Cruz et al. [21]. In their work, they reported that deposited iridium most likely consists of mixed oxides and hydroxides, such as $IrO_{1.1}(OH)_{2.7}{\cdot}0.4H_2O$ and IrO_2. Taking into account the possibility of the presence of IrO_2, there are two possible mechanisms of redox reaction when the pH changes.

$$IrO_2 + 4\,H^+ + 4\,e^- \leftrightarrow Ir + 2\,H_2O$$

$$2\,IrO_2 + 2\,H^+ + 2\,e^- \leftrightarrow Ir_2O_3 + H_2O$$

$$Ir_2O_3 + 6\,H^+ + 6\,e^- \leftrightarrow 2\,Ir + 3\,H_2O$$

This leads to the redox potential according to Equation (1) and subsequently results in a Nernstian response of 59 mV/pH:

$$E = E^0 - 2.303\left(\frac{RT}{nF}\right)\mathrm{pH} = E^0 - 0.059\,\mathrm{pH} \quad (1)$$

where E is the redox potential (in mV), E^0 is the standard electrode potential (in mV), R is the universal gas constant (8.314 $JK^{-1}mol^{-1}$), T is the absolute temperature (in K), F is the Faraday constant (96,485 $Cmol^{-1}$) and n is the number of electrons transferred in the reaction [16,29].

In the presence of oxohydroxides, the following reactions are possible:

$$Ir(OH)_3 \rightarrow Ir(OH)_2O^- + H^+$$

$$Ir_2O(OH)_6 \rightarrow Ir_2O(OH)_3O_3^{3-} + 3\,H^+$$

$$2\,Ir(OH)_3 + H_2O \leftrightarrow Ir_2O(OH)_6 + 2\,H^+ + 2\,e^-$$

$$2\,Ir(OH)_2O^- + H_2O \leftrightarrow Ir_2O(OH)_3O_3^{3-} + 3\,H^+ + 2\,e^-$$

In this case, the response is equal to 88.5 mV/pH [30].

The current and potential dependency of the potentiostatic deposition is shown in Figure 4a. A blank measurement was carried out using a solution with the same pH as the Ir solution, and equal amounts of $C_2H_2O_4{\cdot}2H_2O$, K_2CO_3 and Cl^- ions using NaCl. From the blank measurements, the total charge of the blank experiment was calculated. That

charge is equivalent to the charge of the electrolyte reaction. The total amount of deposited Ir particles was calculated by Faraday's law from the total charge minus the charge from the blank measurement. It was found that the total amount of Ir present on the surface of the samples averaged 0.015 ± 0.007 mg. Figure 2b shows the oxidation process in the physiological solution, which was carried out to oxidize Ir particles on the TiAlV surface.

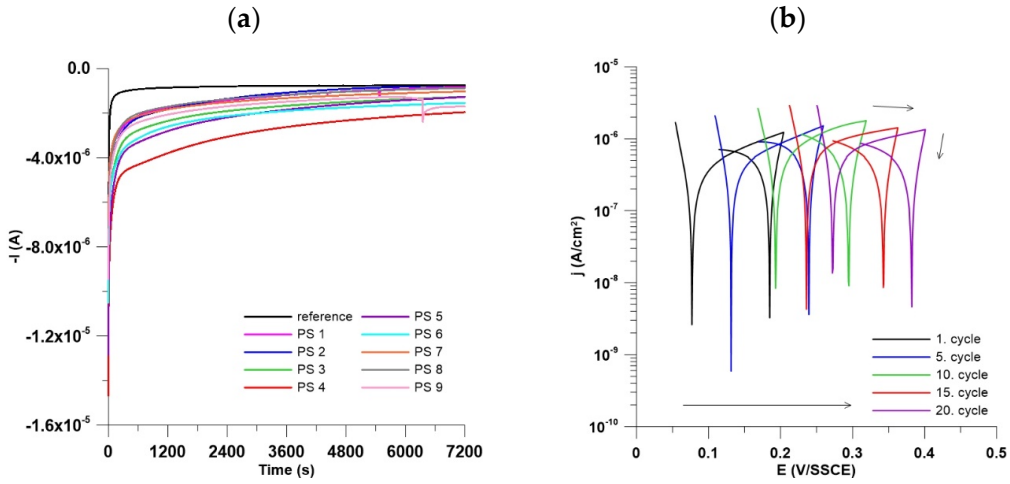

Figure 4. The current and potential dependencies of (**a**) potentiostatic deposition and (**b**) oxidation.

Figure 5a shows Ir PS and Figure 5b displays Ir PS+CP samples. IrO_2 particles were deposited on the samples at the edges of the β-phase cavities and nanotube edges. The diameter of the nanotubes and the width of their walls are summarized in Table 1. The length of the nanotubes was then determined from the TEM image (Figure 5c). These results correspond with those of previously published works [27,31].

Table 1. Diameter, length and wall thickness of nanotube samples Ir PS and Ir PS+CP.

	Nanotube Diameter (nm)	Wall Thickness (nm)	Length (nm)
Ir PS	97.1 ± 7.1	20.9 ± 2.4	429 ± 19
Ir PS+CP	91.0 ± 5.7	19.5 ± 2.5	363.3 ± 8.8

Figure 6 shows the TEM-EDS map of the iridium distribution in the lamella obtained from the (a) Ir PS and (b) Ir PS+CP samples. According to this map, deposited iridium was mainly concentrated on top of the nanotubes in both cases. Only small amounts were detected on the bottom. The main difference between these samples was the amount of Ir detected. Further analyses were subsequently performed to better determine the distribution and the amount of Ir particles.

Figures 7 and 8 show TEM-EDS images with the analyzed areas marked. To confirm the assumption that the deposited Ir occurred predominantly at the tops of the nanotubes, analyses were performed here and at the base of the nanotubes. The results of the analyses are summarized in Tables 2 and 3. The EDS results confirmed that the highest concentration of Ir particles is at the surface of the nanotubes on both samples, while at the same time, the distribution occurs at the bottom of the nanotubes. Platinum was found on the samples from the TEM lamella preparation process, where the surface of the sample is covered with a thin layer of Pt before the lamella is formed and removed, thus protecting the lamella and surrounding area from Ga ions. After the cyclic polarization step, the iridium concentration was reduced as some of it dissolved back into the solution.

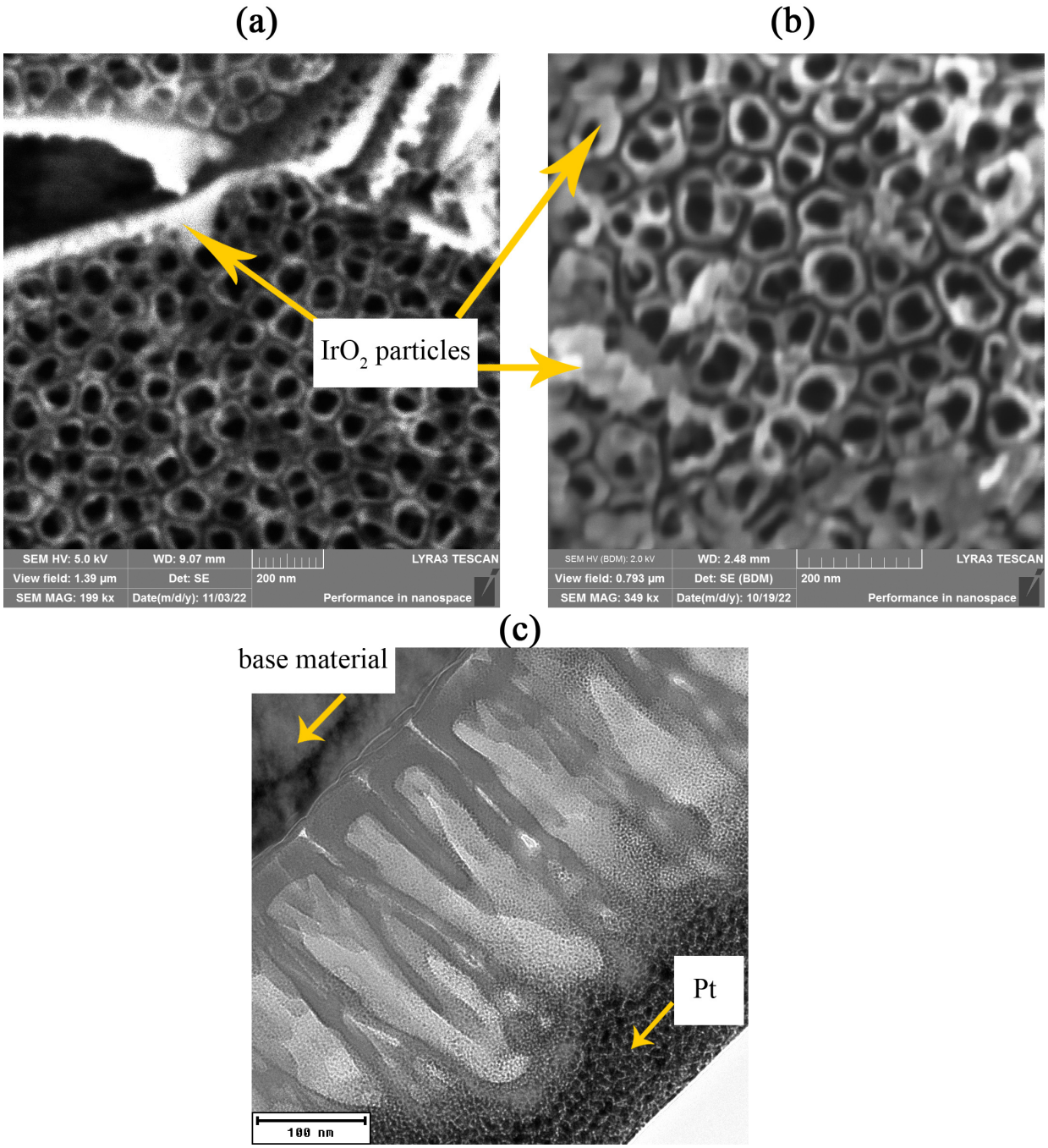

Figure 5. Iridium particles deposited on nanotubes: (**a**) Ir PS (SEM), (**b**) Ir PS+CP (SEM) and (**c**) Ir PS+CP side views of nanotubes (TEM).

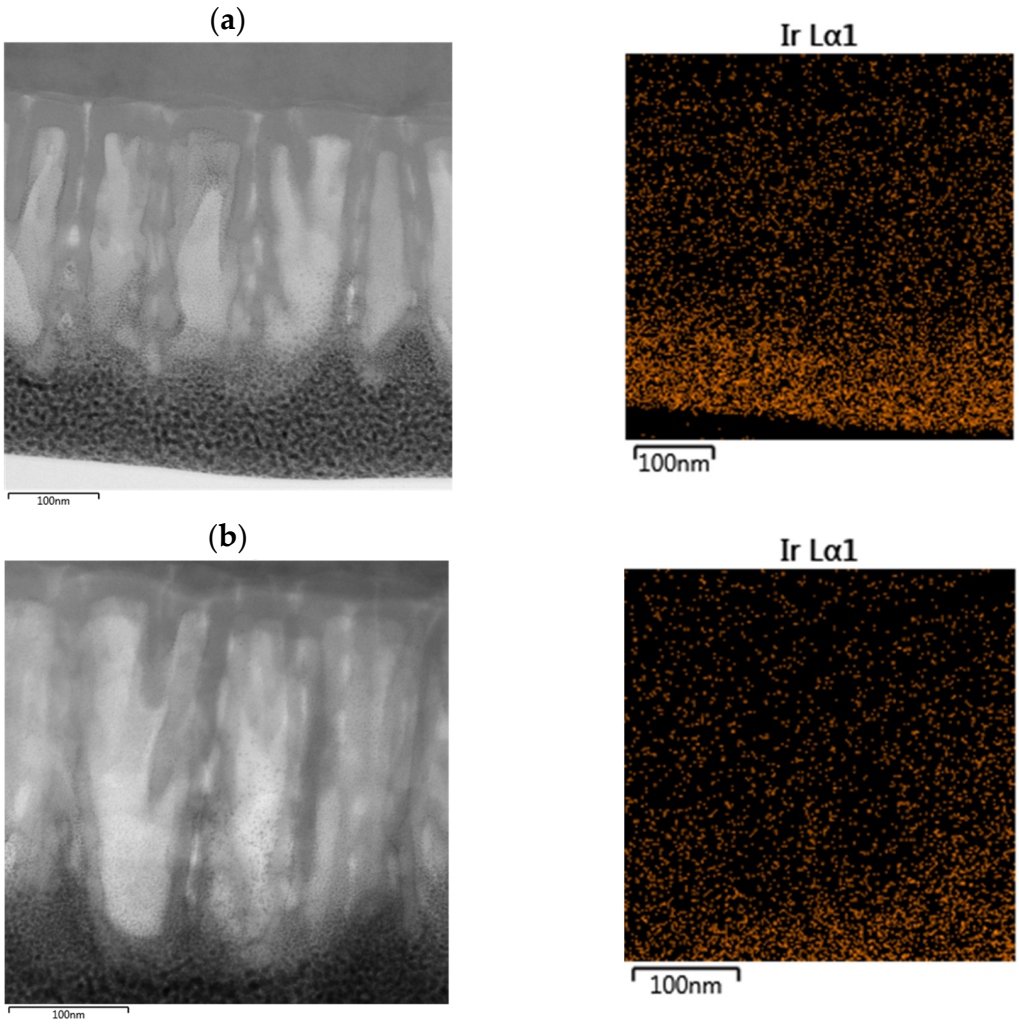

Figure 6. TEM-EDS map of Ir distribution in the lamella from (**a**) Ir PS and (**b**) Ir PS+CP samples.

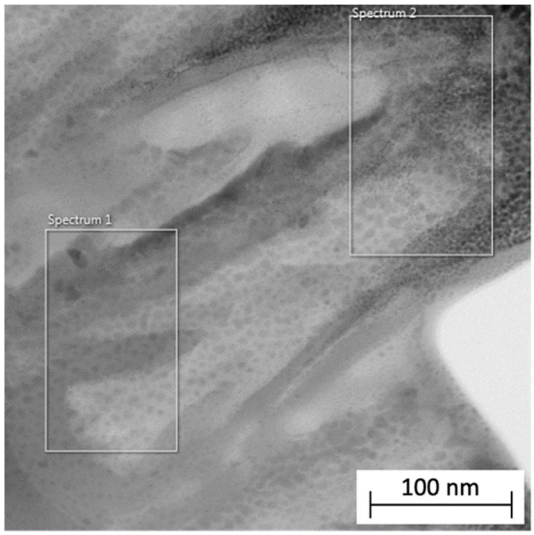

Figure 7. Areas of TEM-EDS analysis of Ir PS for the results shown in Table 2.

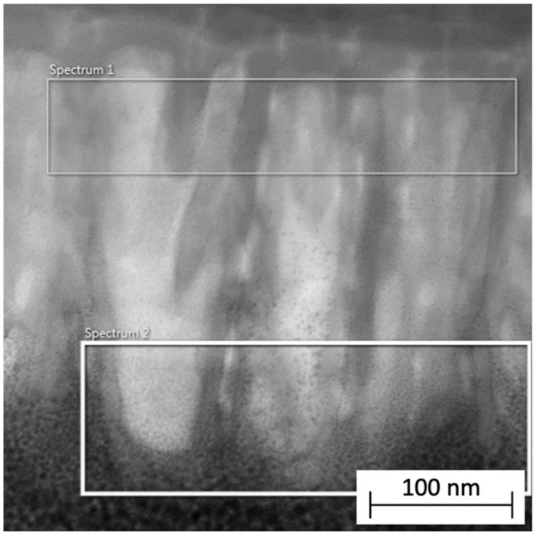

Figure 8. Areas of TEM-EDS analysis of Ir PS+CP for the results shown in Table 3.

Table 2. Results (wt.%) of TEM-EDS analysis of Ir PS.

	Base of Nanotubes (Spectrum 1)	Top of Nanotubes (Spectrum 2)
Ti	84.6 ± 1.2	39.9 ± 0.8
Al	7.0 ± 0.4	3.2 ± 0.2
V	3.4 ± 0.5	1.7 ± 0.3
Ir	4.8 ± 0.9	8.7 ± 0.9
Pt	0.9 ± 0.8	46.6 ± 1.0

Table 3. Results (wt.%) of TEM-EDS analysis of Ir PS+CP.

	Base of Nanotubes (Spectrum 1)	Top of Nanotubes (Spectrum 2)
Ti	85.6 ± 1.3	47.3 ± 1.6
Al	7.9 ± 0.5	4.6 ± 0.5
V	4.4 ± 0.6	2.1 ± 0.5
Ir	2.1 ± 1.3	3.6 ± 1.9
Pt	-	42.3 ± 1.7

Figure 9 displays the iridium distribution profiles obtained by SIMS for both Ir PS and Ir PS+CP samples. The data unequivocally verify that the highest concentration of iridium is localized on the surface of the nanotubes. Remarkably, the iridium content within the remainder of the nanotube structure is nearly identical for both samples. This intentional distribution of iridium throughout the nanotube architecture is crucial for achieving a pH-sensitive surface, as it ensures a uniform exposure of the sensing material to the surrounding environment. This strategic design not only enhances the sensitivity of the sensor but also promotes consistent and reliable pH measurements across the sensor's surface. Compared to previously published works [11,17–19,25,29,30], our presented IrO_2 deposition procedure achieves a reproducible and uniform distribution of particles on the surface of the titanium substrate. By not sealing the nanotubes with Ir particles, the purpose of nanotube formation is preserved, namely to increase the real area compared to the geometric one and maintain the ability to direct biofilm formation detection [27].

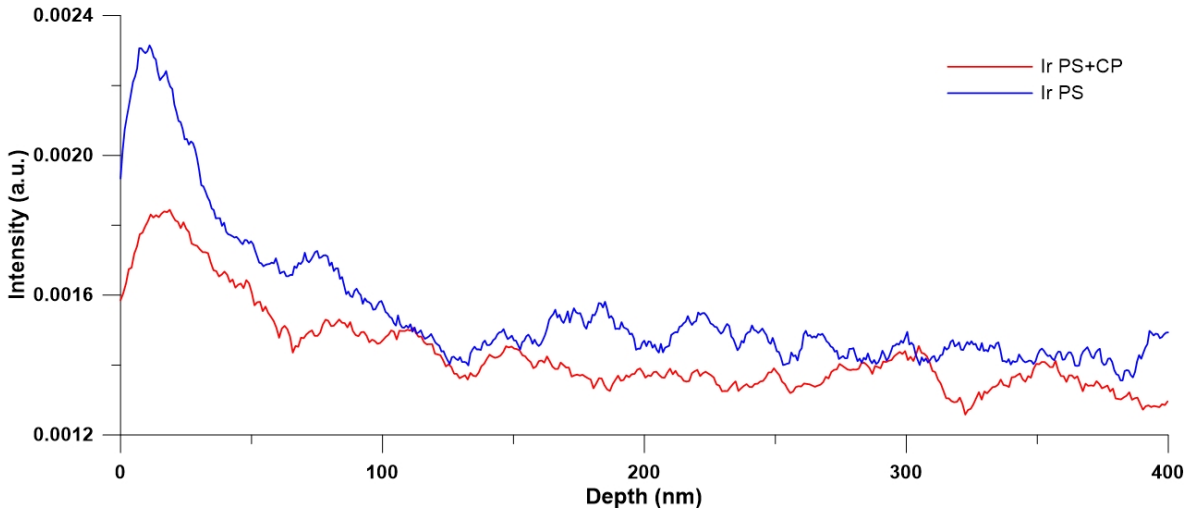

Figure 9. Depth distribution of Ir in Ir PS and Ir PS+CP samples obtained by the SIMS method.

3.3. Electrochemical Response to pH Change

To study the electrochemical response of the sample to the pH change, Ir PS+CP was chosen. The pH range from 6.5 to 7.6 was chosen to reflect the physiological environment with and without inflammation [7]. The first measurements were carried out with the sample, which, after preparation and cleaning, was only kept in a sterile container. The results presented in Figure 10 show that the Ir PS+CP surface responded to the change in pH with a sensitivity of 37 ± 3 mV/pH when the first recorded potential data were taken immediately as the pH decreased. When the data were taken after 5 min, the sensitivity was already 43 ± 3 mV/pH. In order to verify the reliability and stability of the measurements, the experiment was continued with a backward pH increase with the same sample. During the experiment, the hydration of the surface was achieved and the resulting sensitivity was 55 ± 2 mV/pH when the pH was increased.

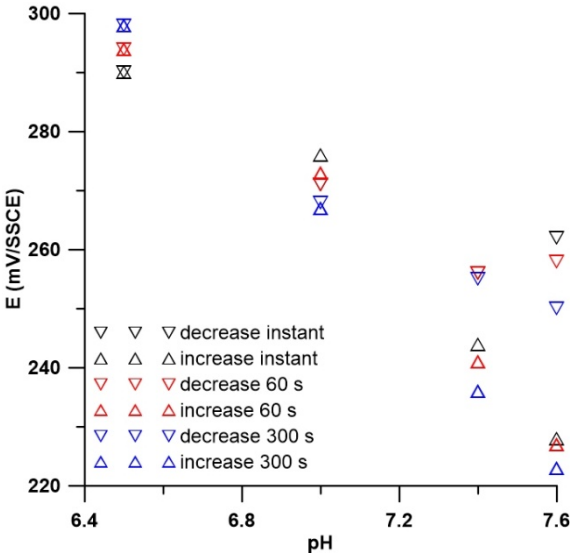

Figure 10. The electrochemical response of Ir PS+CP without initial stabilization.

As the storage medium, the physiological solution with pH 7.6 was chosen. The sample Ir PS+CP was placed in this solution and the potential course was monitored for 40 h (Figure 11). After this time, the surface response to pH change was observed again. Leaving the sample in the storage medium resulted in the hydration of the surface and a more stable response, which was around 45 ± 2 mV/pH for both decreasing and increasing pH values.

The change in pH was recorded by the change in potential immediately after immersion in the solution. However, a better and more stable recording of the electrochemical response was made after 90 s. These data are summarized in Figure 12.

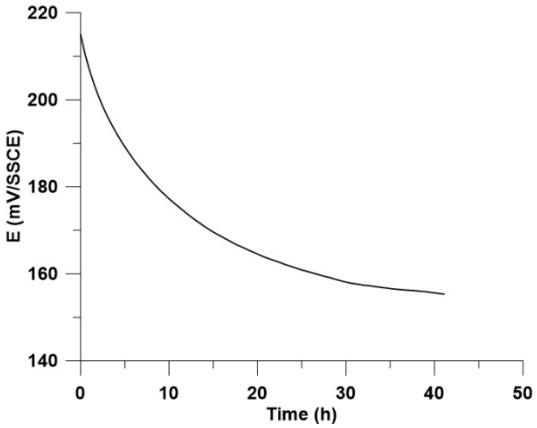

Figure 11. Stabilization of Ir PS+CP sample in a physiological solution at pH 7.6 and 37 °C.

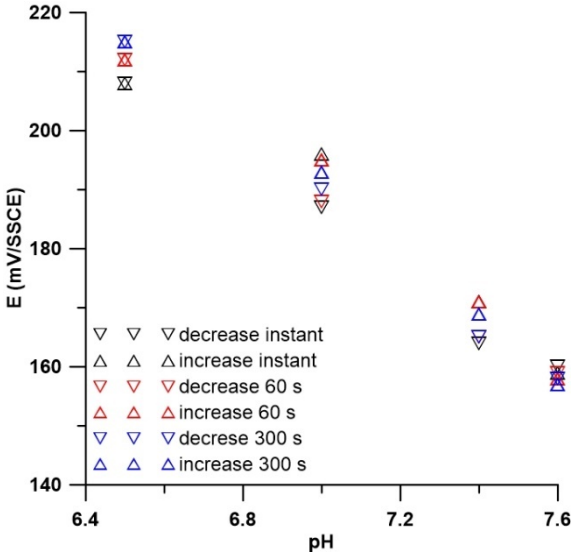

Figure 12. The electrochemical response of Ir PS+CP after 40 h of stabilization.

Another sample was left in the storage medium for 5 days. During that time, the potential course was monitored as an indicator of surface stability (Figure 13). After this time, the electrochemical response was again measured over the selected pH range, as shown in Figure 14. From the first recorded potential value, it was already possible to recognize a change in the pH of the solution. In this case, the surface showed a response of 50 ± 2 mV/pH. If the potential value after 5 min was taken into account, the recording was already stable and the response was 55 ± 1 mV/pH. The electrochemical response analysis of both TiAlV and Ir PS+CP samples reveals intriguing insights into the Nernstian behavior observed in the prepared system. Beyond the contribution of iridium oxides, it becomes apparent that titanium oxides also play a significant role in facilitating the Nernstian response exhibited by the Ir PS+CP sample.

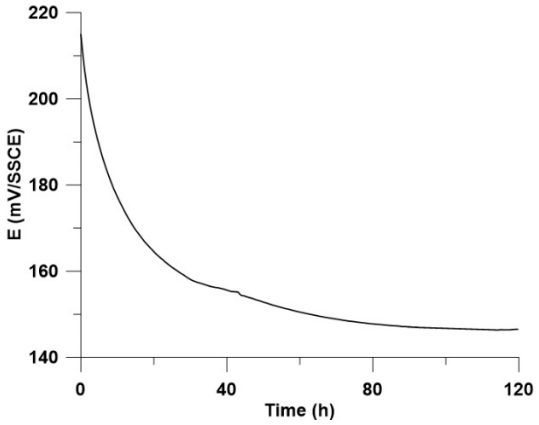

Figure 13. Stabilization of another Ir PS+CP sample in a physiological solution at pH 7.6 and 37 °C.

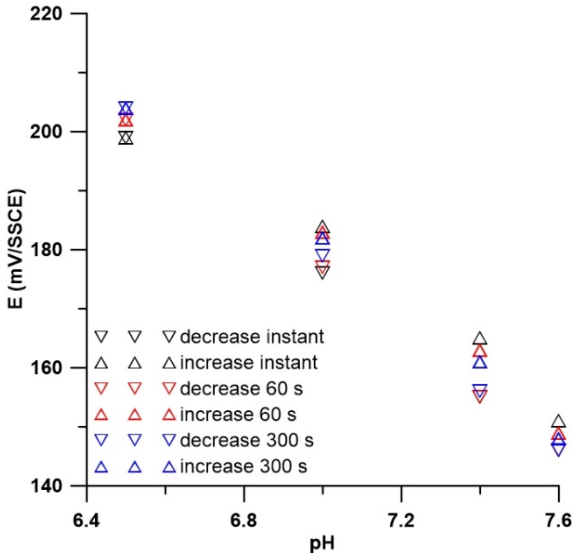

Figure 14. The electrochemical response of Ir PS+CP after 5 days of stabilization.

All previous tests were performed in a 200 mL solution. In the work of Prats-Alfonso et al. [20], the influence of the size of the pH electrode with IrO_2 and their sensitivity was tested. Their work concluded that its size has no effect. On the other hand, the effect of the volume of the tested solution on the sensor response was not tested. In the case of synovial fluid collection in patients with suspected infectious inflammation, specific treatment should be administered. However, in this case, a culture is also needed to determine which bacteria are causing the inflammation around the implant. In this regard, an attempt was made to determine the electrochemical response of the TiO_2-IrO_2 system to a change in pH in a volume of 100 µL. The sample had been in storage solution for a week prior to this experiment. For the detection of pH change, pH values of 7.6 and 6.5 were chosen. Between each measurement, the sample surface was meticulously rinsed with distilled water to mitigate potential contamination and ensure the integrity of subsequent readings, and an SSCE microreference electrode was used as a reference electrode. Remarkably, even within this microvolume setting, the TiO_2-IrO_2 system exhibited remarkable sensitivity to pH changes, with a recorded sensitivity of 55 ± 1 mV/pH. The resulting potential response is shown in Table 4. These results are very positive in view of the intended use in medicine. As discussed in the work of Taheri et al. [16], for pH sensors used in biological environments, rapid response and high sensitivity are very important. An acceptable response to pH change was achieved even in a small volume and short time. Compared to published procedures, potentiostatic deposition appears to be more controllable and economically less demanding [32,33].

Table 4. Results of the pH change monitoring in the microvolume on the surface of Ir PS+CP.

pH	E (mV/SSCE)
7.6	144
6.5	205
7.6	145
6.5	208

Prior to conducting the experiment on the effect of redox potential on the response, the Ir PS+CP sample underwent a preconditioning phase where it was immersed in a storage solution for a week to ensure its stability and consistency. The actual measurement started in a solution of pH 7.6. At the moment when the bubbling of nitrogen started, a potential change was immediately detected at the platinum electrode. In contrast, the prepared Ir PS+CP surface showed no noticeable response to this environmental change. Subsequently, after an hour, when air was reintroduced into the solution, the electrochemical response of Ir PS+CP remained unaffected, contrasting with the detectable changes observed at the platinum electrode. Following this phase, the solution's pH was adjusted to 6.5, prompting an immediate response from the Ir PS+CP sample in accordance with its previously determined sensitivity of 55 ± 1 mV/pH. Approximately 400 s after the pH adjustment, nitrogen bubbling was reintroduced into the solution. Notably, while the platinum electrode exhibited a corresponding change in potential, indicative of its responsiveness to redox fluctuations, no such change was observed for the Ir PS+CP sample. Once the air was reintroduced into the solution, a potential shift was once again recorded for the platinum electrode, while the Ir PS+CP surface maintained its steady electrochemical response. This whole process is summarized in Figure 15.

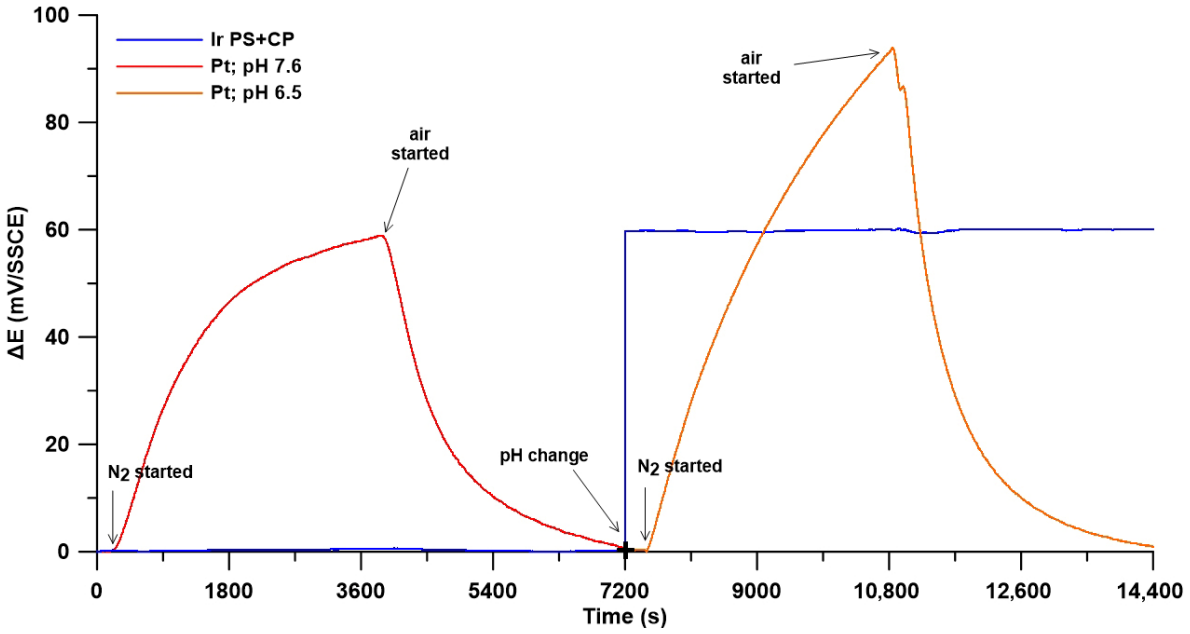

Figure 15. Effect of redox potential on the monitoring of pH change.

From the result of the EDS before and after the exposition (Table 5) of the Ir PS+CP sample, it was proven that there was no dissolution of IrO_2 into the solution during the pH changes. The fluoride listed in the table was a residue from the nanotube preparation that did not affect the sample response. This finding emphasizes the robustness and stability of the IrO_2-based pH sensor and confirms its suitability for prolonged exposure to varying pH conditions without compromising its structural integrity or performance. The absence

of IrO_2 dissolution further supports confidence in the sensor's reliability and longevity, offering valuable insights for its potential applications in diverse environments and scenarios requiring precise pH monitoring capabilities. At the same time, when compared to the work of Liu et al. [17] where both iridium and ruthenium oxides were deposited on a polished titanium substrate, simpler fabrication was achieved with comparable results. At the same time, the preparation of the nanostructure resulted in a much larger real surface area compared to the geometric one, and hence the gain of a larger pH-sensitive surface. The same conclusion was reached in the work by Mingels et al. [19], but here, the iridium oxides were deposited on a platinum electrode with a gold interlayer. The novel potentiostatic process used here for depositing IrO_2 on a titanium substrate without a gold interlayer reduces the fabrication cost without losing the positive properties.

Table 5. Results of EDS analysis (wt.%) of Ir PS+CP before and after exposition in the whole pH range.

	Ti	Al	V	Ir	F
Ir PS+CP before	87.4 ± 1.3	6.1 ± 0.4	4.1 ± 1.4	1.3 ± 0.3	1.1 ± 0.1
Ir PS+CP after	87.3 ± 0.3	6.1 ± 0.3	3.9 ± 0.1	1.3 ± 0.1	1.4 ± 0.2

4. Conclusions

In this work, nanostructured TiAlV alloy samples were successfully prepared. According to the results of the analyses, reproducible potentiostatic deposition of Ir particles was achieved. During oxidation by cyclic polarization in the physiological solution, more stable iridium oxides were obtained on the surface of the Ir PS+CP sample. Based on the SIM and TEM-EDS data, it was found that IrO_2 particles were concentrated on the surface of the nanotubes but also distributed to the bottom of the nanotubes.

Due to the possibility of using the surface immediately after production, our prepared surface is suitable as a pH electrode. During our experiments, the sensitivity of the surface was shown to be 37 ± 3 mV/pH when the surface was used without the storage solution. If the measurement lasted 5 min, the sensitivity was already 43 ± 3 mV/pH. By keeping the sample in the storage solution for 40 h or five days, the surface sensitivity was already 55 ± 1 mV/pH. The electrochemical response in microvolume was measured on another prepared surface which was kept in the physiological solution at pH 7.6 before the experiment. Again, the pH change was successfully detected with the Nernstian sensitivity of 55 ± 1 mV/pH. It was further shown that the mixed surface of TiO_2 and IrO_2 did not respond to the change in the redox potential of the environment. Our experiments showed that the most accurate measurements were obtained when the sensor was kept in a storage solution and readings were taken at least 90 s after immersion. However, it was also possible to use the sensor without a storage medium. This surface with its properties would be suitable for use in medicine, especially for the rapid detection of inflammation in the surrounding area of the implant, when the punctate would be tested.

Author Contributions: Conceptualization, J.F. and A.M.; methodology, J.F. and J.J.; validation, J.F., V.H. and A.M.; formal analysis, J.J., K.K., A.M. and L.K.; investigation, J.J., V.H., A.M. and L.K.; resources, J.J., K.K., A.M. and L.K.; data curation, J.J., V.H. and A.M.; writing—original draft preparation, J.J. and J.F.; writing—review and editing, J.J., V.H., A.M. and J.F.; visualization, J.J.; supervision, J.F. and A.M.; project administration, J.F.; funding acquisition, J.F. All authors have read and agreed to the published version of the manuscript.

Funding: This research was funded by the Czech Health Research Council, grant number NU20-06-00424.

Institutional Review Board Statement: Not applicable.

Informed Consent Statement: Not applicable.

Data Availability Statement: Data are contained within the article.

Conflicts of Interest: The authors declare no conflicts of interest.

References

1. Tomšík, E.; Gunár, K.; Krunclová, T.; Ivanko, I.; Trousil, J.; Fojt, J.; Hybášek, V.; Daniel, M.; Sepitka, J.; Judl, T.; et al. Development of Smart Sensing Film with Nonbiofouling Properties for Potentiometric Detection of Local pH Changes Caused by Bacterial and Yeast Infections around Orthopedic Implants. *Adv. Mater. Interfaces* **2023**, *10*, 2201878. [CrossRef]
2. Busscher, H.J.; van der Mei, H.C.; Subbiahdoss, G.; Jutte, P.C.; van den Dungen, J.J.; Zaat, S.A.; Schultz, M.J.; Grainger, D.W. Biomaterial-associated infection: Locating the finish line in the race for the surface. *Sci. Transl. Med.* **2012**, *4*, 153rv110. [CrossRef] [PubMed]
3. Zhu, Y.; Weng, X.; Zhang, J.; Mao, J. Protective effect of additional cathelicidin antimicrobial peptide PR-39 on prosthetic-joint infections. *J. Orthop. Surg.* **2023**, *31*, 10225536231175237. [CrossRef] [PubMed]
4. Parvizi, J.; Tan, T.L.; Goswami, K.; Higuera, C.; Della Valle, C.; Chen, A.F.; Shohat, N. The 2018 Definition of Periprosthetic Hip and Knee Infection: An Evidence-Based and Validated Criteria. *J. Arthroplast.* **2018**, *33*, 1309–1314.e1302. [CrossRef] [PubMed]
5. Trampuz, A.; Zimmerli, W. Diagnosis and treatment of infections associated with fracture-fixation devices. *Injury* **2006**, *37* (Suppl. S2), S59–S66. [CrossRef] [PubMed]
6. Veletić, M.; Apu, E.H.; Simić, M.; Bergsland, J.; Balasingham, I.; Contag, C.H.; Ashammakhi, N. Implants with Sensing Capabilities. *Chem. Rev.* **2022**, *122*, 16329–16363. [CrossRef] [PubMed]
7. Judl, T.; Popelka, S.; Tomšík, E.; Hrubý, M.; Daniel, M.; Fojt, J.; Melicherčík, P.; Landor, I.; Jahoda, D. Acidity Is an Excellent Marker of Infection in Hip and Knee Arthroplasty. *J. Clin. Med.* **2024**, *13*, 688. [CrossRef] [PubMed]
8. Fisher, C.R.; Masters, T.L.; Johnson, S.; Greenwood-Quaintance, K.E.; Chia, N.; Abdel, M.P.; Patel, R. Comparative transcriptomic analysis of Staphylococcus epidermidis associated with periprosthetic joint infection under in vivo and in vitro conditions. *Int. J. Med. Microbiol.* **2024**, *315*, 151620. [CrossRef] [PubMed]
9. Rotstein, O.D.; Nasmith, P.E.; Grinstein, S. The Bacteroides by-product succinic acid inhibits neutrophil respiratory burst by reducing intracellular pH. *Infect. Immun.* **1987**, *55*, 864–870. [CrossRef]
10. Rotstein, O.D.; Pruett, T.L.; Fiegel, V.D.; Nelson, R.D.; Simmons, R.L. Succinic acid, a metabolic by-product of Bacteroides species, inhibits polymorphonuclear leukocyte function. *Infect. Immun.* **1985**, *48*, 402–408. [CrossRef]
11. Shahrestani, S.; Ismail, M.C.; Kakooei, S.; Beheshti, M.; Zabihiazadboni, M.; Zavareh, M.A. Iridium Oxide pH Sensor Based on Stainless Steel Wire for pH Mapping on Metal Surface. *IOP Conf. Ser. Mater. Sci. Eng.* **2018**, *328*, 012014. [CrossRef]
12. Widmer, A.F. New Developments in Diagnosis and Treatment of Infection in Orthopedic Implants. *Clin. Infect. Dis.* **2001**, *33*, S94–S106. [CrossRef] [PubMed]
13. McLister, A.; McHugh, J.; Cundell, J.; Davis, J. New Developments in Smart Bandage Technologies for Wound Diagnostics. *Adv. Mater.* **2016**, *28*, 5732–5737. [CrossRef] [PubMed]
14. Gray, M.; Meehan, J.; Ward, C.; Langdon, S.P.; Kunkler, I.H.; Murray, A.; Argyle, D. Implantable biosensors and their contribution to the future of precision medicine. *Vet. J.* **2018**, *239*, 21–29. [CrossRef] [PubMed]
15. Singewald, T.D.; Traxler, I.; Schimo-Aichhorn, G.; Hild, S.; Valtiner, M. Versatile, low-cost, non-toxic potentiometric pH-sensors based on niobium. *Sens. Bio-Sens. Res.* **2022**, *35*, 100478. [CrossRef]
16. Taheri, M.; Deen, I.A.; Packirisamy, M.; Deen, M.J. Metal oxide -based electrical/electrochemical sensors for health monitoring systems. *TrAC Trends Anal. Chem.* **2024**, *171*, 117509. [CrossRef]
17. Liu, B.; Zhang, J. A ruthenium oxide and iridium oxide coated titanium electrode for pH measurement. *RSC Adv.* **2020**, *10*, 25952–25957. [CrossRef] [PubMed]
18. Marzouk, S.A.M. Improved Electrodeposited Iridium Oxide pH Sensor Fabricated on Etched Titanium Substrates. *Anal. Chem.* **2003**, *75*, 1258–1266. [CrossRef] [PubMed]
19. Mingels, R.H.G.; Kalsi, S.; Cheong, Y.; Morgan, H. Iridium and Ruthenium oxide miniature pH sensors: Long-term performance. *Sens. Actuators B Chem.* **2019**, *297*, 126779. [CrossRef]
20. Prats-Alfonso, E.; Abad, L.; Casan-Pastor, N.; Gonzalo-Ruiz, J.; Baldrich, E. Iridium oxide pH sensor for biomedical applications. Case urea-urease in real urine samples. *Biosens. Bioelectron.* **2013**, *39*, 163–169. [CrossRef]
21. Cruz, A.M.; Abad, L.; Carretero, N.M.; Moral-Vico, J.; Fraxedas, J.; Lozano, P.; Subías, G.; Padial, V.; Carballo, M.; Collazos-Castro, J.E.; et al. Iridium Oxohydroxide, a Significant Member in the Family of Iridium Oxides. Stoichiometry, Characterization, and Implications in Bioelectrodes. *J. Phys. Chem. C* **2012**, *116*, 5155–5168. [CrossRef]
22. Zhao, R.; Xu, M.; Wang, J.; Chen, G. A pH sensor based on the TiO_2 nanotube array modified Ti electrode. *Electrochim. Acta* **2010**, *55*, 5647–5651. [CrossRef]
23. Awad, N.K.; Edwards, S.L.; Morsi, Y.S. A review of TiO_2 NTs on Ti metal: Electrochemical synthesis, functionalization and potential use as bone implants. *Mater. Sci. Eng. C Mater. Biol. Appl.* **2017**, *76*, 1401–1412. [CrossRef] [PubMed]
24. Benea, L.; Ravoiu, A.; Neaga, V.; Axente, E.R. Using Applied Electrochemistry to Obtain Nanoporous TiO_2 Films on Ti_6Al_4V Implant Alloys and Their Preclinical In Vitro Characterization in Biological Solutions. *Coatings* **2023**, *13*, 614. [CrossRef]
25. Machackova, N.; Jiru, J.; Hybasek, V.; Fojt, J. A Ru/RuO2-Doped TiO2 Nanotubes as pH Sensors for Biomedical Applications: The Effect of the Amount and Oxidation of Deposited Ru on the Electrochemical Response. *Materials* **2021**, *14*, 7912. [CrossRef]
26. Moravec, H.; Vandrovcova, M.; Chotova, K.; Fojt, J.; Pruchova, E.; Joska, L.; Bacakova, L. Cell interaction with modified nanotubes formed on titanium alloy Ti-6Al-4V. *Mater. Sci. Eng. C* **2016**, *65*, 313–322. [CrossRef]
27. Fojt, J.; Průchová, E.; Hybášek, V. Electrochemical impedance response of the nanostructured Ti–6Al–4V surface in the presence of S. aureus and E. coli. *J. Appl. Electrochem.* **2023**, *53*, 2153–2167. [CrossRef]

28. Saharudin, K.A.; Sreekantan, S.; Aziz, S.N.Q.A.A.; Hazan, R.; Lai, C.W.; Mydin, R.B.S.M.N.; Mat, I. Surface Modification and Bioactivity of Anodic Ti6Al4V Alloy. *J. Nanosci. Nanotechnol.* **2013**, *13*, 1696–1705. [CrossRef]
29. Kim, T.Y.; Yang, S. Fabrication method and characterization of electrodeposited and heat-treated iridium oxide films for pH sensing. *Sens. Actuators B Chem.* **2014**, *196*, 31–38. [CrossRef]
30. Dong, L.; Qiu, Y.; Gu, Y.; Wang, Y.; Li, L. Preparation of an iridium oxide micro pH electrode and its response rate under dynamic stray current interference. *Microchem. J.* **2024**, *196*, 109631. [CrossRef]
31. Jiang, P.; Zhang, Y.; Hu, R.; Shi, B.; Zhang, L.; Huang, Q.; Yang, Y.; Tang, P.; Lin, C. Advanced surface engineering of titanium materials for biomedical applications: From static modification to dynamic responsive regulation. *Bioact. Mater.* **2023**, *27*, 15–57. [CrossRef]
32. Manjakkal, L.; Szwagierczak, D.; Dahiya, R. Metal oxides based electrochemical pH sensors: Current progress and future perspectives. *Prog. Mater. Sci.* **2020**, *109*, 100635. [CrossRef]
33. Jang, H.; Lee, J. Iridium oxide fabrication and application: A review. *J. Energy Chem.* **2020**, *46*, 152–172. [CrossRef]